HHS Public Access

Author manuscript

Int Symp Med Robot. Author manuscript; available in PMC 2022 September 19.

Published in final edited form as:

Int Symp Med Robot. 2022 April ; 2022: . doi:10.1109/ismr48347.2022.9807517.

Delta Robot Kinematic Calibration for Precise Robot-Assisted Retinal Surgery

Boyang Xiao,
LCSR at the Johns Hopkins University, Baltimore, MD 21218 USA

Alireza Alamdar,
LCSR at the Johns Hopkins University, Baltimore, MD 21218 USA

Kefan Song,
LCSR at the Johns Hopkins University, Baltimore, MD 21218 USA

Ali Ebrahimi,
LCSR at the Johns Hopkins University, Baltimore, MD 21218 USA

Peter Gehlbach [Member, IEEE],
Wilmer Eye Institute, Johns Hopkins Hospital, Baltimore, MD 21287 USA

Russell H. Taylor [Life Fellow, IEEE],
LCSR at the Johns Hopkins University, Baltimore, MD 21218 USA

Iulian Iordachita [Senior Member, IEEE]
LCSR at the Johns Hopkins University, Baltimore, MD 21218 USA

Abstract

High precision is required for ophthalmic robotic systems. This paper presents the kinematic calibration for the delta robot which is part of the next generation of Steady-Hand Eye Robot (SHER). A linear error model is derived based on geometric error parameters. Two experiments with different ranges of workspace are conducted with laser sensors measuring displacement. The error parameters are identified and applied in the kinematics to compensate for modeling error. To achieve better accuracy, Bernstein polynomials are adopted to fit the error residuals after compensation. After the kinematic calibration process, the error residuals of the delta robot are reduced to satisfy the clinical requirements.

I. Introduction

Vitreoretinal microsurgery is challenging due to the constrained workspace and extremely high accuracy requirements. Human hands are limited in terms of tremor and precision in manipulating surgical tools [1]. To reconcile these problems, a number of medical robotic systems with the ability to cancel tremor, and with sensor-servo functions have been developed [2].

bxiao4@jhu.edu .

At the present time, there have been three broad classes of ophthalmic robots developed: handheld robots, teleoperated robots, and cooperative-control robots [3]. A handheld robot is directly held and manipulated by surgeons. It has fewer degrees of freedom (DOFs), smaller dimensions and simpler mechanisms, which make it less expensive and more intuitive in clinical applications [2]. The Micron system developed by Carnegie Mellon University is one of the most referenced handheld robot systems [4]. The AID [5] and *ITrem* [6] also belong in this category. The other class are teleoperated robots consisting of a patient-side robot and a user interface. Surgeons can manipulate the robot remotely with the benefit of motion scaling and tremor-free control. The Preceyes from Eindhoven University of Technology, which is able to improve precision by 10 to 20 times that of human hands, is well-known in this field [7]. This robotic system has been used in clinical applications. Another example is the master-slave robotic system developed by the University of Tokyo [8]. It has attained successful microvascular cannulation in an *ex-vivo* experiment. In cooperative-control robotic system class, the surgeon and the robot share control of surgical tools. The robotics manipulator from the University of Leuven is a typical cooperative-control system [9]. The Steady-Hand Eye Robot (SHER) developed by Johns Hopkins University also falls into this category [10].

The SHER is a 5-DOF cooperative-control system. While the operator is manipulating the shared surgical tool, the operator's hand forces exerted on the robot are sensed by force/torque sensors mounted on the tool, multiplied by a controller gain factor, and converted to desired velocity command of the robot end-effector. In this way, the robot can move precisely and in the absence of physiological tremor. The newest generation of SHER is shown in Fig. 1. This robotic platform consists of a 3-DOF stage based on a delta robot structure, and a 2-DOF robotic arm supporting a compact tool holder with a quick-release mechanism and a surgical tool. The delta robot and the robotic arm are connected serially, which means the accuracy of the delta robot can be independently analyzed to contribute to the entire robot precision. In this paper, we focus on the resulting improvement in accuracy of the surgical tool tip for subretinal injections. It is assumed that all the rotary motions are performed prior to the needle insertion process, thus only the Cartesian motion defined by the delta robot contributes to the accuracy during this process. Therefore, this paper focuses solely on the precision improvement of the delta robot.

The robotic system is subject to many sources of error, including machine tolerances, assembly errors, structural deformations, backlash, and component wear. Some of these errors are constant which means they could be reduced through kinematic calibration. To achieve accuracy improvement, an error model is needed. Common methods, including the product of exponential (POE) method and the vector loop method, may be used for error modeling [11]. These methods have been applied to parallel mechanics such as delta robots resulting in improved performance [12]. After parameter identification, the error can be compensated via the kinematics. In addition, a stiffness model can be introduced into the kinematic calibration process [11]. To acquire better results, some numerical methods such as polynomial fitting can be applied with the kinematic calibration [13].

In our study, the contribution is twofold. First, a linear error model with geometric error parameters for the delta robot is derived and combined with a Bernstein polynomial model

for correction. Second, experiments for kinematic calibration are then conducted to identify the parameters and coefficients of these two models and reduce the error residuals following compensation.

II. Methods

The SHER system is developed here in order to assist ophthalmologists in providing therapy to the subretinal domain which is the space between the internal limiting membrane (ILM) and the retinal pigment epithelium (RPE) cells layer [2]. The proposed positional accuracy requirement for this robotic system is 20 μm, which is more precise than the clinical accuracy of 25–30 μm needed for subretinal injections [2]. To achieve this proposed precision, the machining and assembly errors of the delta robot are minimized, followed by a kinematic calibration. The kinematic calibration workflow is shown in Fig. 2. First, the linear error model is derived using Jacobian matrix based on the selection of error parameters. Second, the error parameters are identified according to the experiment data. Then, the error can be compensated by applying identified parameters in the kinematics. Lastly, the error residuals after compensation are fitted by a Bernstein polynomial to further improve the accuracy of the delta robot.

A. Error Modeling and Parameter Identification

A vector loop method is used for error modeling since the delta robot is a parallel mechanism. Fig. 3 shows a 3-D view of the delta robot used in the SHER. It is composed of a base platform, a moving platform and three limbs. Each limb is built by two parallel rods and spherical joints. The moving platform remains parallel to the base platform because of this parallelogram mechanism. For the error model, the limbs are simplified as $\underline{\boldsymbol{P}}UU$ limbs, where $\underline{\boldsymbol{P}}$ represents the active prismatic joint and U represents the universal joint. The base frame $\{\boldsymbol{O}\}$ is attached to the center of the base platform, and the end-effector frame $\{\boldsymbol{O}'\}$ is attached to the center of moving platform. The orientation of the base frame and the end-effector frame always remains the same due to the parallelogram configuration. The Cartesian displacement of the moving platform are defined by x, y, z. For those three limbs, the nominal prismatic joint values are L_i (i = 1, 2, 3). The nominal distances between the base frame and the prismatic joint are r_{bi}. The nominal distances between end-effector frame and the universal joint are r_{pi}. The relative angles for the prismatic joints on the base platform are θ_{bi} with respect to the base frame. The relative angles for the universal joints on the moving platform are θ_{pi} with respect to the end-effector frame. The nominal length of the limbs is l_i. The joint values of three prismatic joints are q_i. The i-th vector loop closure equation is given by

$$\boldsymbol{r} = \boldsymbol{r}_{bi} + \boldsymbol{L}_i + \boldsymbol{l}_i - \boldsymbol{r}_{pi}, \tag{1}$$

where $\boldsymbol{r} = [x, y, z]^{\mathrm{T}}$, $\boldsymbol{r}_{bi} = [r_{bi}\cos\theta_{bi}, r_{bi}\sin\theta_{bi}, 0]^{\mathrm{T}}$, $\boldsymbol{r}_{pi} = [r_{pi}\cos\theta_{pi}, r_{pi}\sin\theta_{pi}, 0]^{\mathrm{T}}$, and $\boldsymbol{L}_i = [0, 0, q_i]^{\mathrm{T}}$. All the vectors are expressed in the base frame $\{\boldsymbol{O}\}$. Based on (1), the length of the limb l_i can be written as

$$l_i^2 = \|\boldsymbol{l}_i\|^2 = \|\boldsymbol{r} + \boldsymbol{r}_{bi} - \boldsymbol{r}_{pi} - \boldsymbol{L}_i\|^2 . \tag{2}$$

The scalar form of (2) is

$$x^2 + y^2 + z^2 + 2a_i x + 2b_i y - 2q_i z + c_i = 0, \tag{3}$$

where $a_i = r_{pi} \cos\theta_{pi} - r_{bi} \cos\theta_{bi}$, $b_i = r_{pi} \sin\theta_{pi} - r_{bi} \sin\theta_{bi}$ and $c_i = a_i^2 + b_i^2 + q_i^2 - l_i^2$.

To derive the error model, all the geometric error sources are chosen as error parameters. As the source errors are much smaller than the nominal values, the first-order approximation of (3) is formulated by

$$2[(x + a_i)\Delta x + (y + b_i)\Delta y + (z - q_i)\Delta z + x\Delta a_i + y\Delta b_i - z\Delta q_i] + \Delta c_i = 0, \tag{4}$$

Where

$$\Delta a_i = \cos\theta_{pi}\,\Delta r_{pi} - r_{pi} \sin\theta_{pi}\,\Delta\theta_{pi} - \cos\theta_{bi}\,\Delta r_{bi} + r_{bi} \sin\theta_{bi}\Delta\theta_{bi}, \tag{5}$$

$$\Delta b_i = \sin\theta_{pi}\,\Delta r_{pi} + r_{pi} \cos\theta_{pi}\,\Delta\theta_{pi} - \sin\theta_{bi}\Delta r_{bi} - r_{bi} \cos\theta_{bi}\Delta\theta_{bi}, \tag{6}$$

$$\Delta c_i = 2a_i\Delta a_i + 2b_i\Delta b_i + 2q_i\Delta q_i - 2l_i\Delta l_i\,. \tag{7}$$

Substituting (5)–(7) into (4) and rewriting the equations result in the linearized error model of delta robot

$$\Delta \boldsymbol{r} = \begin{pmatrix} \Delta x \\ \Delta y \\ \Delta z \end{pmatrix} = \boldsymbol{J}_a(q_i)\Delta \boldsymbol{p}_a, \tag{8}$$

where $\boldsymbol{J}_a$ is a 3×18 Jacobian matrix and $\Delta\boldsymbol{p}_a$ is an 18×1 vector including all the errors of the geometric parameters Δr_{bi}, Δr_{pi}, $\Delta\theta_{bi}$, $\Delta\theta_{pi}$, Δq_i, Δl_i.

Before identifying error parameters, their identifiability needs to be verified. After assigning arbitrary joint values, the rank of the Jacobian matrix $\boldsymbol{J}_a$ is calculated. By checking the dependence of each two rows, Δr_{bi} and Δr_{pi} are found to be dependent. $\Delta\theta_{bi}$ and $\Delta\theta_{pi}$ are found to be dependent as well. The final error model without redundant parameters can be written as

$$\Delta \boldsymbol{r} = \begin{pmatrix} \Delta x \\ \Delta y \\ \Delta z \end{pmatrix} = \boldsymbol{J}(q_i)\Delta \boldsymbol{p}, \tag{9}$$

where $\boldsymbol{J}$ is a 3×12 Jacobian matrix and $\Delta\boldsymbol{p} = [\Delta r_{b1}, \Delta\theta_{b1}, \Delta q_1, \Delta l_1, \ldots, \Delta r_{b3}, \Delta\theta_{b3}, \Delta q_3, \Delta l_3]^{\mathrm{T}}$ is a 12×1 vector.

To identify the error parameters, the identification equation can be constructed as

$$\delta \boldsymbol{r}_* = \boldsymbol{J}_*\Delta \boldsymbol{p}, \tag{10}$$

where $\Delta \boldsymbol{r}_* = \left[\Delta \boldsymbol{r}_1^{\mathrm{T}}, \Delta \boldsymbol{r}_2^{\mathrm{T}}, \ldots, \Delta \boldsymbol{r}_n^{\mathrm{T}}\right]^{\mathrm{T}}$, which is built by stacking the end-effector positional error at n different configurations and $\boldsymbol{J}_* = \left[\boldsymbol{J}_1^{\mathrm{T}}, \boldsymbol{J}_2^{\mathrm{T}}, \ldots, \boldsymbol{J}_n^{\mathrm{T}}\right]^{\mathrm{T}}$, which is built by stacking the corresponding Jacobian matrices. The least square algorithm can be adopted to solve for the parameters. The objective function could be expressed as

$$\underset{\delta \boldsymbol{p}}{\operatorname{argmin}} \left\| \delta \boldsymbol{r}_* - \boldsymbol{J}_* \Delta \boldsymbol{p} \right\|. \tag{11}$$

The identified parameters can be applied in kinematics to achieve the accuracy improvement referred to as the Jacobian method.

B. Bernstein Polynomial Correction

Due to several reasons, the error residuals compensated by the Jacobian method may not meet the accuracy requirements. In order to achieve better accuracy, a Bernstein polynomial is applied to correct the residuals. Compared to the power-based polynomial, the Bernstein polynomial has better numerical stability and robustness [14]. The model we use can be expressed as

$$BP(x_d, y_d, C, n) = \sum_{j=0}^{n} \sum_{k=0}^{n} \left[C_{j,k} \binom{n}{k} \binom{n}{j} {x_d}^k (1 - x_d)^{n-k} {y_d}^j (1 - y_d)^{n-j} \right], \tag{12}$$

where x_d and y_d are desired end-effector position calculated by the forward kinematics, n is the order of the Bernstein polynomial, $C_{j,k}$ is the undetermined coefficient, and C is a matrix including all $(n+1)^2$ coefficients. To fit the Bernstein polynomial, the input x_d and y_d are required to be normalized. The end-effector position z is not introduced in this model to prevent overfitting since the horizontal performance of the delta robot is assumed to be the same among different levels. Different Bernstein polynomials are used to fit the error in three directions. The Levenberg-Marquardt algorithm is applied to fit the coefficients because of its good performance in non-linear least square problems [15]. The objective function is written as

$$\underset{C}{\operatorname{argmin}} \left\| e_{jac} - BP(x_d, y_d, C, n) \right\|, \tag{13}$$

where e_{jac} represents the error residual compensated by Jacobian method in one direction.

III. EXPERIMENT

To implement the kinematic calibration method proposed in the previous section, the desired position from forward kinematics and the actual position from the external measurement are required. In this case, the experiments are conducted on the prototype of the delta robot.

The setup is shown in Fig. 4. The prismatic joints of the delta robot are controlled with a Galil motion controller (DMC-4183, Galil Motion Control, Rocklin, CA) through three servomotors (Maxon RE25 10 W, Maxon Precision Motors, Inc., USA) and three magnetic linear absolute encoders (RLS, LA11DCB13BKA30DF00, 13-bit resolution, Renishaw,

Inc., West Dundee, IL). The controller is connected to a PC and the Galil Design Kit software is used to send control commands and record absolute encoder data. Three laser sensors (Keyence LK-H157, range 150±40 mm, linearity ±1.6 μm, Keyence Corporation of America, Itasca, IL), which are connected to the laser control box, are used for obtaining the 3-D position of the moving platform. To reduce measurement error and the noise of sensors, an aluminum calibration cube with smooth surface and good perpendicularity (4×4×2 in, Tight-Tolerance Multipurpose 6061 Aluminum, McMaster-Carr Supply Company, Elmhurst, IL) is mounted on the moving platform of the delta robot.

The available workspace for the delta robot is a cylinder with the radius of 27.5 mm and the height of 40 mm. In clinical application, the SHER will be used with a human operator in a loop containing real-time microscope image feedback. Surgeons will start to manipulate the robot from somewhere in the workspace until the tool tip reaches the target. To accomplish the therapeutic maneuver in the subretinal domain, the robot is expected to be more accurate in the region of interest (ROI) on the retina. Since the human eye is approximately a 25 mm sphere in diameter [2], the ROI of this robot is defined as a 20×20×20 mm cube in the center of the workspace and the center point of the ROI is defined as the home position. In this case, two experiments are designed and conducted. The first experiment is the whole workspace calibration. Three horizontal planes with a height of −20, 0, 20 mm relative to the home position are selected. In each plane, 14×14 grid points are tested for the delta robot. The moving range is from −20 mm to 20 mm in both the x and y directions. The second experiment is the local workspace calibration directed at the ROI. Similarly, three horizontal planes with a height of −10, 0, 10 mm are chosen, and 11×11 grid points are selected in each plane to be tested. The moving range is from −10 mm to 10 mm in both x and y directions.

Before the experiment, the reference position is set as the position where the moving platform and the base platform are concentric. The experiment starts with commanding the delta robot to the assigned position and staying for two seconds. The absolute encoder data and laser sensor data are recorded at the same time. For each configuration, the joint values are found from the encoder data, and the actual position of the moving platform is acquired using the difference of laser sensor readings between current position and reference position. The same experiment is repeated five times to check the repeatability of the delta robot. After the experiment, data for 588 poses of the whole workspace calibration and 393 poses of the local workspace calibration are collected. After converting the raw data to joint values and actual positions, the error of one pose can be calculated by

$$e_0 = \begin{pmatrix} e_{x0} \\ e_{y0} \\ e_{z0} \end{pmatrix} = \begin{pmatrix} x_m \\ y_m \\ z_m \end{pmatrix} - F(L_i), \tag{14}$$

where x_m, y_m, z_m are measured positions in x, y, z direction and $F(L_i)$ is forward kinematics output.

IV. RESULTS AND DISCUSSION

To assure that the kinematic calibration can be applied to this robot, the repeatability of two experiments is checked. The repeatability of motion in three directions for each point is calculated and the average in x, y, z for the whole workspace calibration experiment is ±19.1 μm, ±14.9 μm, and ±14.5 μm respectively. For the local workspace calibration experiment, the average in x, y, z is ±3.7 μm, ±5.4 μm, and ±4.1 μm respectively.

To apply the kinematic calibration algorithm, the error residuals in x, y, z for all the configurations are calculated using (14). The results of two calibration experiments in one horizontal plane ($z = 0$) are shown in Fig. 5. The results indicate that the error varies smoothly in the workspace. The RMS error and standard deviation for all the points in two experiments are shown in Table 1. To compare the performance of different experiments, the RMS error of the whole workspace calibration in the ROI ($x, y \in [-10,10]$ mm) is also calculated. The overall pattern and variation trends are consistent between different experiment methods.

With the error residuals of each pose and corresponding joint values, the error parameters for two experiments can be identified by least square algorithm with the objective function (11). The identified parameters are shown in Table 2, which can be applied to the forward kinematics. The error residuals after compensation are shown in Fig. 6 and the RMS errors are listed in Table 1. For Jacobian method, the performance in the middle of the workspace is better than overall workspace and is close to the result of local workspace calibration as expected. Comparing the results before and after calibration, except from some outliers at the extreme positions, the error is significantly reduced by 5 to 10 times. The Jacobian method successfully captures the majority of the error sources using a simple error model with 12 parameters. However, the result after compensation doesn't meet the proposed requirement of 20 μm. One possible reason is that some conditions assumed in the error model are not satisfied. For example, the moving platform and the base platform might not stay parallel while moving. Another possible reason is that some measurement error, such as the misalignment between the laser beams and the surfaces of the calibration cube, are not being considered. Through the observation of the trend in the residual error, the polynomial correction is adopted over the Jacobian method.

The data from only one horizontal plane are used in the fitting process to prevent overfitting. The inputs of the Bernstein polynomial are normalized desired position calculated from the joint values, and the output is the error residuals compensated by Jacobian method. The data set is randomly split into three parts, 70% for training, 20% for validation, and 10% for testing [16]. The coefficients of the polynomial with different orders are solved by Levenberg-Marquardt algorithm with the objective function (13). The Bernstein polynomials from 2nd to 6th order are considered since the higher order polynomial may cause overfitting [17]. The final adopted model is chosen by finding the polynomial with the best performance which is defined as the lowest RMS error on the validation set. The model choice and RMS error of the test set are given in Table 3. To further validate the performance of this method and the assumption that the delta robot has the same performance between different horizontal planes, the trained models are also applied to the

error residuals from the other two horizontal planes that are not used for fitting. After the Bernstein polynomial correction, the error is further reduced for the two experiments. For the whole workspace calibration, the performance of the different levels are not consistent, which may verify the assumption that the moving platform and the base platform are not always parallel. The local workspace calibration has more accurate and more consistent performance in a smaller workspace as compared to the whole workspace calibration. The error residuals are reduced to less than 20 μm. To get better performance in the surgical tool tip accuracy, it is recommended to use the error parameters and Bernstein polynomial of the local workspace calibration when the tool tip is inside the region of interest. When the tool tip is outside the region of interest, using the error parameters and Bernstein polynomial of the whole workspace calibration is recommended. Since the cooperative control strategy is adopted for this robot, applying the error parameters to the Jacobian matrix of the joint velocities could also improve the control performance.

Finally, by applying the Jacobian method and Bernstein polynomial correction, we achieved a reduction in error by two orders of magnitude in the center of the workspace, thereby meeting the proposed accuracy requirement for clinical application.

V. Conclusion

Through this study, the following points have been achieved:

- A linear error model containing 12 independent geometric error parameters and a Bernstein polynomial model are proposed for the kinematic calibration of the delta robot to improve the accuracy of a cooperative-control ophthalmic robotic system.
- Two experimental methods having different ranges of workspace for the delta robot are conducted using three laser sensors to measure the external positions.
- The 12 geometric error parameters are identified using least square algorithm on the datasets for both whole workspace and local workspace calibration. After the compensation by error parameters, the error residuals are reduced by on the order of 5 to 10 times.
- The Bernstein polynomial is applied to fit the error residuals after the Jacobian method. The undetermined parameters are solved by the Levenberg-Marquardt algorithm. After compensation, the RMS error for the local workspace calibration is reduced to less than 20 μm following kinematic calibration, which now meets the accuracy requirement for the clinical application.

Future work including verification of the delta robot kinematic calibration, kinematic calibration of the robotic arm as well as analysis of resolution and rigidity for the whole robot will be performed to achieve the functional purposes of this new SHER system.

Acknowledgment

Under a license agreement between Galen Robotics, Inc and the Johns Hopkins University, Russell H. Taylor and Johns Hopkins University are entitled to royalty distributions on technology that may possibly be related to that discussed in this publication. Russell H. Taylor also is a paid consultant to and owns equity in Galen Robotics,

Inc. This arrangement has been reviewed and approved by the Johns Hopkins University in accordance with its conflict-of-interest policies.

Research supported by U.S. National Institutes of Health under grant number 1R01EB025883-01A1 and JHU internal funds.

References

[1]. Wei Tech Ang, Riviere CN and Khosla PK, "Design and implementation of active error canceling in hand-held microsurgical instrument," Proceedings 2001 IEEE/RSJ International Conference on Intelligent Robots and Systems. Expanding the Societal Role of Robotics in the Next Millennium (Cat. No.01CH37180), vol.2, pp. 1106–1111, 2001, doi: 10.1109/IROS.2001.976316.

[2]. Vander Poorten E, Riviere CN, Abbott JJ, Bergeles C, Nasseri MA, Kang JU, Sznitman R, Faridpooya K and Iordachita I, "Robotic retinal surgery," Handbook of Robotic and Image-Guided Surgery, pp. 627–672, 2020, doi: 10.1016/B978-0-12-814245-5.00036-0.

[3]. Channa R, Iordachita I and Handa JT, "Robotic Vitreoretinal Surgery," Retina (Philadelphia, Pa.), vol. 37, pp. 1220–1228, July 2017, doi: 10.1097/IAE.0000000000001398.

[4]. MacLachlan RA, Becker BC, Tabares JC, Podnar GW, Lobes LA and Riviere CN, "Micron: An Actively Stabilized Handheld Tool for Microsurgery," in IEEE Transactions on Robotics, vol. 28, no. 1, pp. 195–212, Feb. 2012, doi: 10.1109/TRO.2011.2169634. [PubMed: 23028266]

[5]. Saxena A and Patel RV, "An active handheld device for compensation of physiological tremor using an ionic polymer metallic composite actuator," 2013 IEEE/RSJ International Conference on Intelligent Robots and Systems, 2013, pp. 4275–4280, doi: 10.1109/IROS.2013.6696969.

[6]. Latt WT, Tan U, Shee CY and Ang WT, "A compact hand-held active physiological tremor compensation instrument," 2009 IEEE/ASME International Conference on Advanced Intelligent Mechatronics, pp. 711–716, 2009, doi: 10.1109/AIM.2009.5229927.

[7]. Meenink T, Naus G, de Smet M, Beelen M, and Steinbuch M, "Robot assistance for micrometer precision in vitreoretinal surgery," Investigative ophthalmology & visual science, vol. 54, no. 15, pp. 5808–5808, 2013.

[8]. Ida Y, Sugita N, Ueta T, Tamaki Y, Tanimoto K and Mitsuishi M, "Microsurgical robotic system for vitreoretinal surgery," Int J CARS, vol. 7, pp. 27–34, 2012, doi: 10.1007/s11548-011-0602-4.

[9]. Gijbels A, Wouters N, Stalmans P, Van Brussel H, Reynaerts D and Poorten EV, "Design and realisation of a novel robotic manipulator for retinal surgery," 2013 IEEE/RSJ International Conference on Intelligent Robots and Systems, pp. 3598–3603, 2013, doi: 10.1109/IROS.2013.6696869.

[10]. Mitchell B, Koo J, Iordachita I, Kazanzides P, Kapoor A, Handa J, Hager G and Taylor R, "Development and Application of a New Steady-Hand Manipulator for Retinal Surgery," Proceedings 2007 IEEE International Conference on Robotics and Automation, pp. 623–629, 2007, doi: 10.1109/ROBOT.2007.363056.

[11]. Mei B, Xie F, Liu X and Yang C, "Elasto-geometrical error modeling and compensation of a five-axis parallel machining robot," Precision Engineering, vol. 69, pp. 48–61, 2021, doi: 10.1016/j.precisioneng.2021.01.007.

[12]. Bai P, Mei J, Huang T and Chetwynd DG, "Kinematic calibration of Delta robot using distance measurements," Proceedings of the Institution of Mechanical Engineers, Part C: Journal of Mechanical Engineering Science, vol. 230, no. 3, pp. 414–424, 2016, doi: 10.1177/0954406215603739.

[13]. Feng L, Wilkening P, Sevimli Y, Balicki M, Olds KC and Taylor RH, "Accuracy assessment and kinematic calibration of the robotic endoscopic microsurgical system," 2016 38th Annual International Conference of the IEEE Engineering in Medicine and Biology Society (EMBC), pp. 5091–5094, 2016, doi: 10.1109/EMBC.2016.7591872.

[14]. Farouki Rida T., "The Bernstein polynomial basis: A centennial retrospective," Computer Aided Geometric Design, vol. 29, pp. 379–419, 2012, doi: 10.1016/j.cagd.2012.03.001.

[15]. Gavin HP, "The Levenberg-Marquardt algorithm for nonlinear least squares curve-fitting problems," Department of Civil and Environmental Engineering, Duke University, pp. 1–19, 2019.

[16]. Hastie T, Tibshirani R and Friedman JH, "The elements of statistical learning: data mining, inference, and prediction," vol. 2, New York: springer, 2009.

[17]. Prautzsch H, Boehm W and Paluszny M, "Bézier and B-spline techniques," vol. 6, Berlin: Springer, 2002.

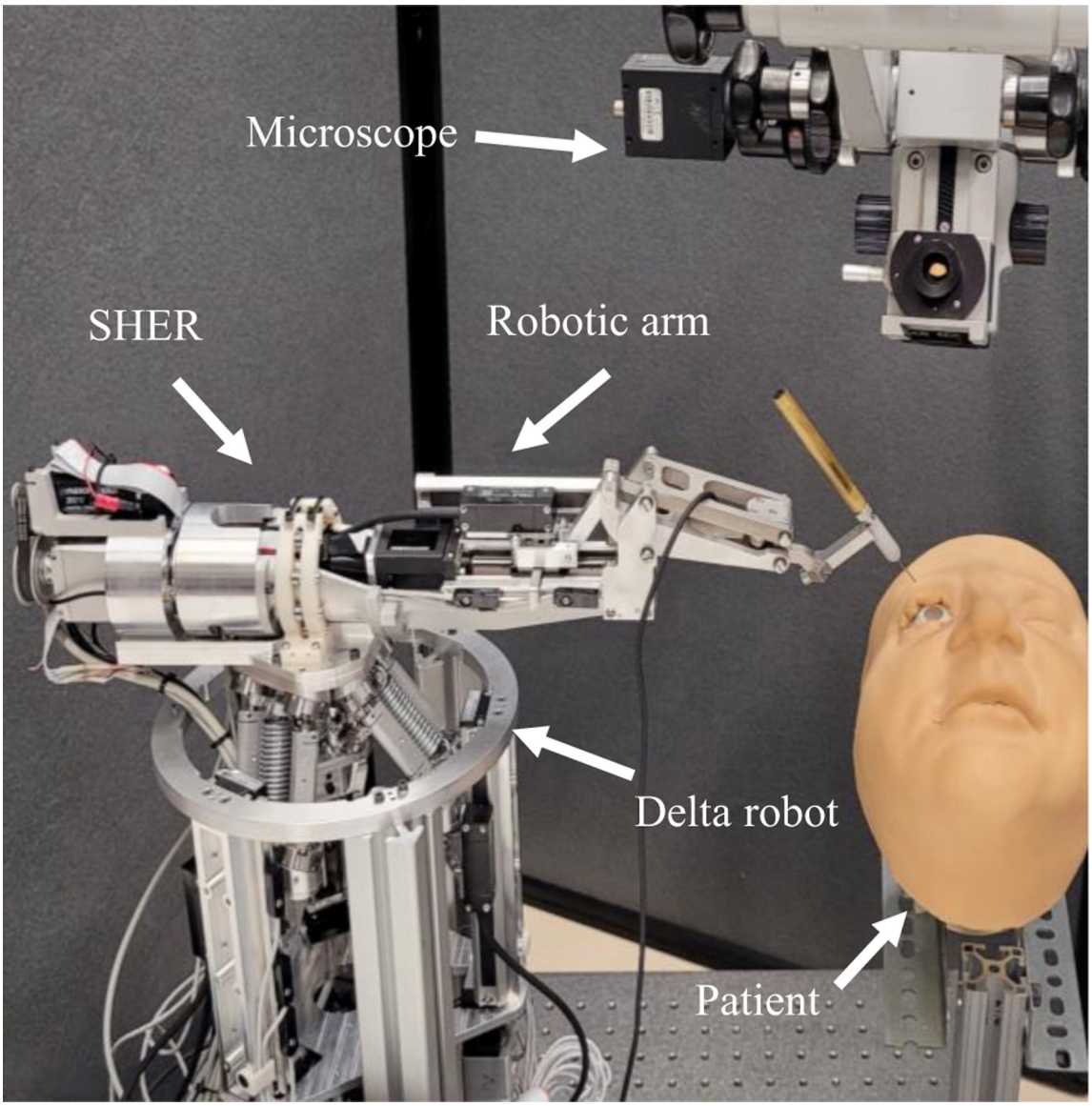

Figure. 1.
Demonstration of the clinical setup of the new SHER system

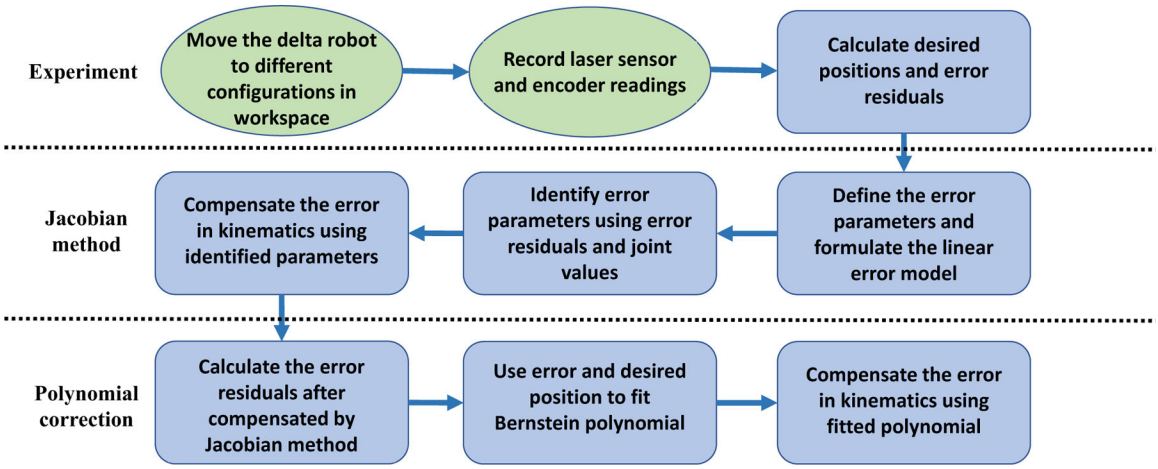

Fig. 2.

Workflow of the delta robot kinematic calibration. The green blocks are experiment steps, the blue blocks are analytical steps

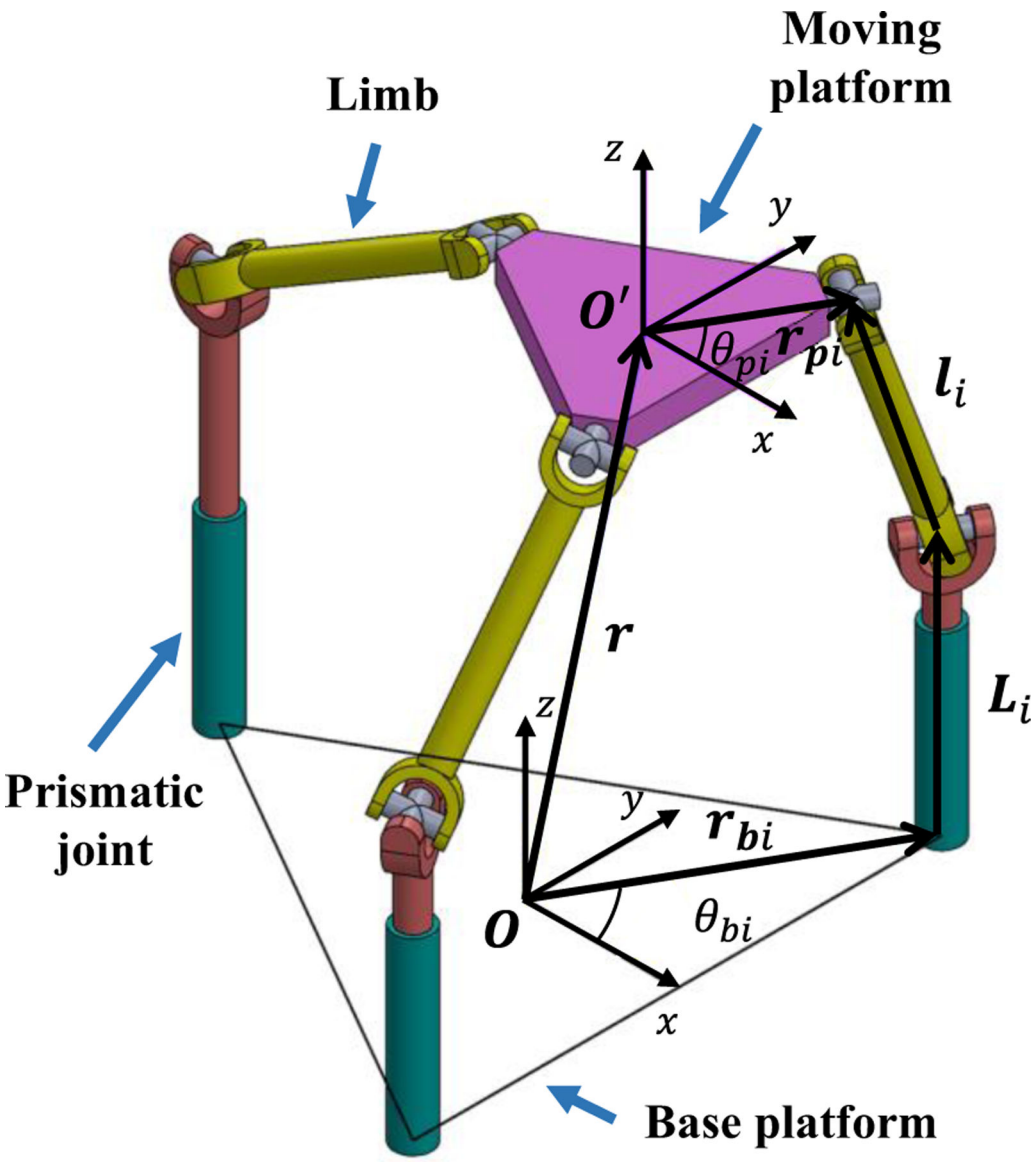

Fig. 3.
3-D view of the delta robot

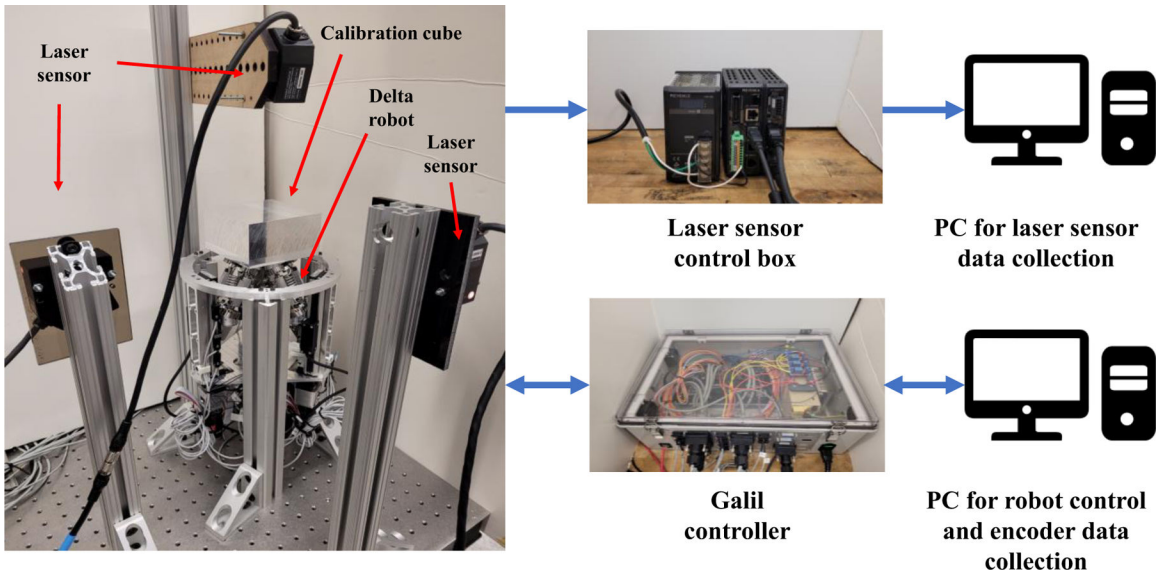

Fig. 4.
Experiment setup of kinematic calibration

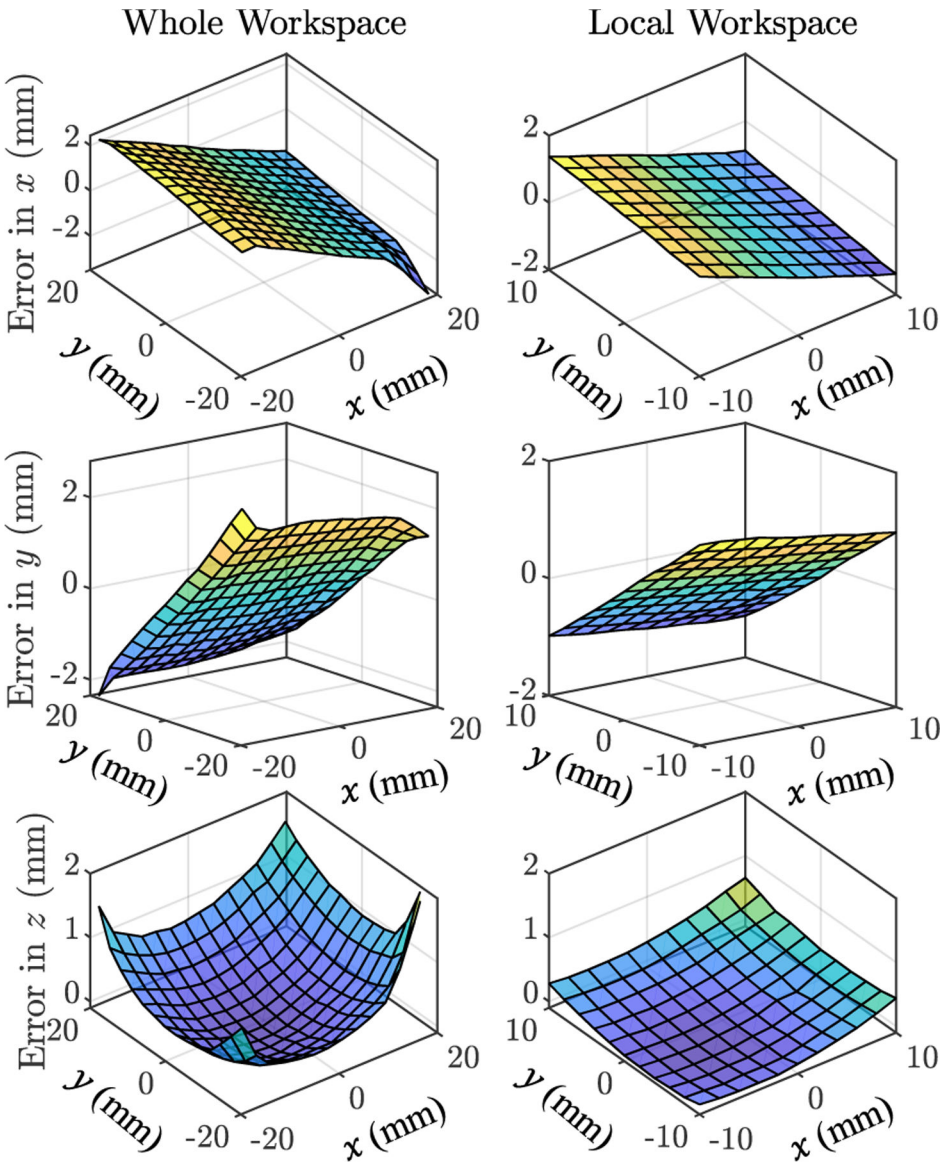

Fig. 5.

Error residuals in *x*, *y*, *z* direction of the whole workspace calibration (*left*) and the local workspace calibration (*right*) before calibration at the height of 0 mm

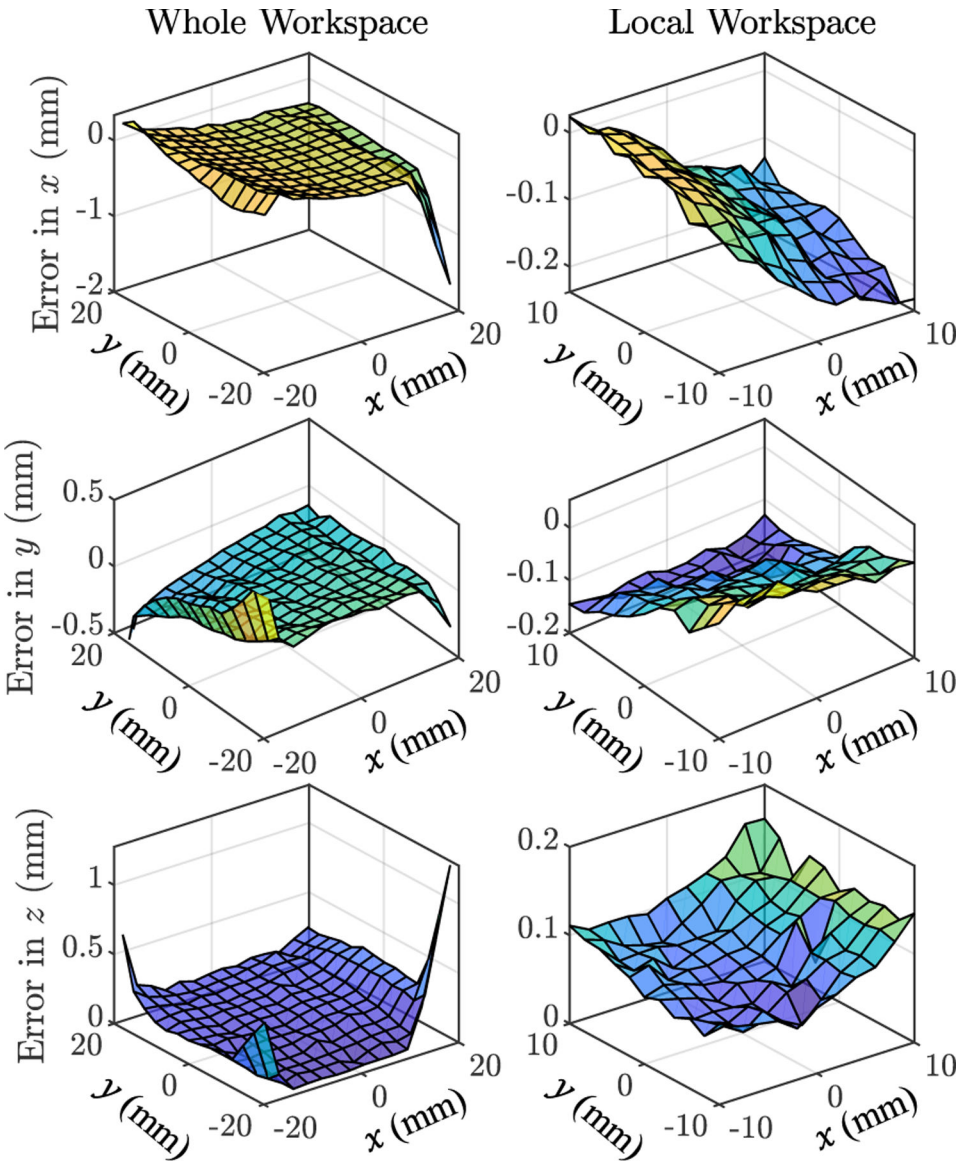

Fig. 6.

Error residuals in *x*, *y*, *z* direction of the whole workspace calibration (*left*, *scale = 0.5mm for error*) and the local workspace calibration (*right*, *scale = 0.1mm for error*) after compensated by error parameters at the height of 0 mm

TABLE I.

Error residuals before and after applied jacobian method

Error (μm)	Whole Workspace Calibration				Local Workspace Calibration	
	Before calibration	*After applied Jacobian method*	*Before calibration (ROI)*	*After applied Jacobian method (ROI)*	*Before calibration*	*After applied Jacobian method*
x	1388±1390	245±217	798±780	140±74	762±764	121±68
y	1293±1297	149±144	769±771	77±66	771±773	97±57
z	650±459	217±149	175±149	116±34	222±169	100±27

Int Symp Med Robot. Author manuscript; available in PMC 2022 September 19.

TABLE II.

IDENTIFIED ERROR PARAMETERS

i	Whole Workspace				Local Workspace			
	δr_{bi} (mm)	$\delta\theta_{bi}$ (deg)	δL_i (mm)	δl_i (mm)	δr_{bi} (mm)	$\delta\theta_{bi}$ (deg)	δL_i (mm)	δl_i (mm)
1	−2.31	0.38	−0.43	1.23	1.33	0.12	1.31	−0.70
2	5.19	0.21	−1.79	3.49	3.76	0.15	1.28	0.28
3	2.83	−1.32	0.68	0.44	2.57	−1.83	1.60	−0.49

TABLE III.

Error residuals after applied polynomial correction

Error (μm)	Whole Workspace Calibration						Local Workspace Calibration			
	Order	***Test set* (z = 0)**	**z = 20**	**z = −20**	**z = 20 *(ROI)***	**z = −20 *(ROI)***	***Order***	***Test set* (z = 0)**	**z = 10**	**z = −10**
x	6	40±38	121±80	82±75	72±4	35±1	3	**11±10**	**18±18**	**18±18**
y	6	27±28	36±35	90±49	23±1	88±3	3	**9±9**	**15±15**	**16±16**
z	6	31±31	77±76	27±25	46±2	11±1	3	**13±12**	**18±15**	**13±13**